Landslides (2019) 16:2277–2286
DOI 10.1007/s10346-019-01251-2
Received: 18 April 2019
Accepted: 24 July 2019
Published online: 3 August 2019

Alex Sanzeni · Marco Peli · Stefano Barontini · Francesco Colleselli

Modelling of an accidentally triggered shallow landslide in Northern Italy

Abstract The paper presents a case study of a landslide event, accidentally triggered by an unexpected and extraordinary infiltration in an otherwise stable slope. The work aims at modelling the slope failure mechanism with a simplified two-dimensional framework based on the formation of a perched water table. The landslide occurred in Val Venosta/Vinschgau Valley, in Northern Italy, in April 2010 and produced catastrophic consequences. It took place on a hillside with average slope angle 36° and affected an area of about 200 m^2; the slip surface was located approximately 1.0 m below the slope profile, in the uppermost layers of a predominantly coarse, well-graded soil. A series of numerical simulations were performed to back-analyse the event, using a commercial computer program. The artificial water infiltration and water content evolution were modelled with a two-dimensional finite element model (FE) of the unsaturated/saturated domain with appropriate infiltration boundary conditions. The slope stability analyses were conducted with a classic limit equilibrium method (LE) and were performed at different time instants during the infiltration process. The soil-water retention curves and conductivity functions were defined according to the van Genuchten-Mualem model. The combined FE and LE simulations showed the gradual formation of a perched water table, whose associated localized pore pressure distribution resulted in the loss of the suction stabilizing effect and thus in the reduction of the safety factor. Although supported by basic soil mechanical and hydraulic characterization, the numerical simulations allowed to perform a back-analysis which effectively captured the timing of the event and the location and depth of the slip surface along the slope.

Keywords Landslide · Infiltration · Modelling · Back-Analysis

Introduction

The present work is focused on the interpretation of the mechanisms involved in the failure of an infiltration-triggered shallow landslide, accidentally occurred in April 2010 in Val Venosta/Vinschgau Valley (Province of Bolzano, South Tyrol, in Northern Italy). The event took place as a consequence of an unexpected infiltration of a fairly great amount of water from a malfunctioning irrigation system located upstream, affecting an area of approximately 200 m^2 in an otherwise stable hillside, with average slope angle of 36°. Although the landslide dimensions were small, its consequences were catastrophic because it caused the loss of nine lives and the injury of 28 people, and it significantly damaged the local railway infrastructure.

There is a large body of literature regarding the occurrence of shallow landslides in Italy and in the world, either induced by natural events or artificially promoted (see Bogaard and Greco 2016, 2018 for an extensive review on this topic). For example, Moser and Hohensinn (1983) presented a detailed investigation of 140 slope movements recorded in Upper Carinthia and Eastern Tyrol (Austria, near to the location of the present case study), which occurred during rather different precipitation events. The majority of failure events took place in the hillside cover soils (colluvial and residual soils with almost equal amounts of gravel, sand and silt), never exceeding 1- to 2-m depth. Similar experiences were reported by Cancelli and Nova (1985) for failure events taking place in Valtellina (Central Italian Alps). Another notable series of landslides triggered in hillside covers occurred in May 1998 in Campania (Southern Italy). These events took place after several days of small intensity rain, in shallow deposits of colluvial, weathered and pyroclastic soil and were analysed and modelled by Cascini et al. (2010, 2011) and by Mancarella et al. (2012). However, the two groups of researchers presented different interpretations and modelling to explain the triggering mechanisms. While Cascini et al. (2010) associated the occurrence of such events to rainfall that directly infiltrated from the slope surface and from the underlying rock, Mancarella et al. (2012) observed that the failure surface of events at the highest altitudes was generally located within the pyroclastic mantle and therefore focused on the potential role of capillary barriers in the formation of a perched water table. Capillary barriers are soil layers characterized by great hydraulic conductivity and small attitude to retain water, which in unsaturated conditions may inhibit water percolation. Askarinejad et al. (2012) created two full-scale field tests on a steep forested slope that was intensively investigated with in situ and laboratory tests, instrumented and monitored over a period of 6 months in the course of artificial rainfall and natural precipitation. The experimental data were used to explain the behaviour of a marginally stable slope by means of two- and three-dimensional stability calculations. Similarly, Springman et al. (2013) presented a 2-year monitoring experiment conducted on a slope in shallow weathered soils, overlying a sandstone bedrock. The researchers measured relatively great values of suction near the ground surface (up to 90 kPa) and evidences of perched water table onset were collected. According to Tarantino and Bosco (2000), the occurrence of shallow landslides may be associated either only to the loss of suction-related apparent cohesion in steep slopes (i.e. when the slope angle is greater than the effective friction angle) or to the progressive increase of positive pore water pressure in gentle slopes. As a threshold between steep and gentle slopes, the authors suggested slope angles ranging from 35° to 40°, which is the case of many shallow landslides occurred in the Alpine region, as observed by Moser and Hohensinn (1983). The transition between unsaturated and saturated soil may frequently generate a perched water table, which is a confined saturated zone within unsaturated soil, and occurs due to the presence of a relatively less conductive layer typically with greater fine content. The coarser soil below this finer layer behaves as a capillary barrier and prevents water from infiltrating downward (Shackelford et al. 1994). This happens because the lower coarser layer is non-conductive at great suction, so the upper layer is

forced to behave as a container and to store infiltrating water until it reaches a value of matric suction that matches with the capillary pore diameter of the coarser layer (Khire et al. 2000).

This paper, which develops and deepens a previous preliminary study presented at the 4th World Landslide Forum (Sanzeni et al. 2017), describes the case study and presents the numerical simulations that were conducted to analyse the event. The modelling was carried out with SLIDE 6.0 computer software (Rocscience Inc. 2010). The software is capable of performing infiltration and seepage simulations in the saturated and unsaturated domain, and slope stability analyses with limit equilibrium methods, which adopt the pore pressure distribution generated by the infiltration analyses. The boundary conditions during the infiltration were defined as an application of the model of perched water table proposed by Barontini et al. (2015). A number of stability calculations were executed at prescribed time steps during infiltration to appreciate the evolution of the safety factor and to reconstruct the intensity-duration function of the slope according to the model proposed by Caine (1980).

The case study

The landslide occurred in Val Venosta/Vinschgau Valley (Province of Bolzano, South Tyrol, Northern Italy) in April 2010 on a natural slope that was formed as the result of the erosion produced by the flow of the Adige River on the cone of an alluvial deposit. The event affected an area of about 200 m^2 in the central part of a hillside with average inclination of approximately 36°. The slip surface (approximate length 20 m, width from 8 to 12 m) was located about 1.0 m below the slope profile, in the uppermost layers of a predominantly coarse, well-graded soil (Fig. 1a). The event was triggered by an accidental and extraordinary infiltration of water from a malfunctioning component of an irrigation system located on the uphill flat area (Fig. 1b). Although the slope appears to be uniformly covered with vegetation, the landslide apparently occurred in an area where there were no trees. After the occurrence of the event, a number of activities were performed to characterize the area (before the authors' involvement). A geotechnical investigation campaign was carried out which consisted of three boreholes (Fig. 1b), with SPT and hydraulic conductivity tests, some exploration trenches and geophysical testing. In the course of the campaign, a number of soil samples were collected from the boreholes, from the area of the landslide and from the mobilized soil. The samples of soils were subjected to standard laboratory classification tests to determine particle size distribution and plasticity. Precipitation and temperature data from the nearby Schlanders/Silandro meteorological station were also collected to investigate the antecedent water content conditions.

Strategy of the numerical simulation

The back-analysis of the event was conducted with the computer software SLIDE (Rocscience Inc. 2010), capable of performing finite element (FE) simulations of the transient infiltration-seepage process in the saturated-unsaturated domain. The pore pressure distribution generated by the FE simulation during the infiltration was adopted for the execution of stability analyses with the (simplified) limit equilibrium (LE) method developed by Bishop (1955), with unbound position of the centre of the slip surfaces. The LE method was applied to slip surfaces deeper than 1.0 m, in order to avoid the necessity of simulating the effect of a superficial soil layer with vegetation roots (grass and bushes). This modelling strategy, based on uncoupled numerical simulations, has already been successfully adopted in the literature (Cascini et al. 2010, 2011; Askarinejad et al. 2012; Springman et al. 2013; Barla et al. 2013; Ozbay and Cabalar 2015).

Geometrical features

The slope is 65 m long, 36° steep, topped with an almost flat area, where the irrigation system (the source of water infiltration) was located (Fig. 1b). The numerical simulations were conducted on a simplified scheme, as represented in Fig. 2a. The uphill flat area was considered irrelevant for understanding the hydrological and geotechnical behaviour of the slope, and therefore, it was neglected. The soil is a coarse alluvial deposit, covered by an on-average 1.5 m thick (in the transverse direction) predominantly silty-sandy layer. In the following, we will refer to L1 as to the silty-sandy soil layer, and to L2 as to the coarse alluvial deposit. According to the observations conducted in the field after the event, the presence of trees and vegetation was not considered in any way in the model (in fact, no trees were involved in the landslide). The numerical model is an unstructured mesh of triangular elements with varying fineness (Fig. 2b). The mesh is coarser at the bottom of the model (about 6 elements over 10 m of boundary), and finer along the slope where the landslide occurred (about 12 elements over 10 m of boundary). The 2D model did not account for the effect of the three-dimensional geometry of the landslide. However, this topic was investigated by Askarinejad et al. (2012), who extended the two-dimensional equilibrium analysis of a slope to a three-dimensional geometry with laterally limited sides, in order to account for the resisting forces along the sides of the failure wedge. For a failure event with very similar features to the case presented in this study, the researchers estimated a 10% increase in safety factor from 2D to 3D model.

Geotechnical properties

The mechanical properties of the soils on the slope were estimated by interpreting the results of the geotechnical investigation and in situ tests conducted after the event and before the author's involvement. Figure 3 presents the particle size distribution of three samples collected from the slope near the slip surface and shows the different composition of the soil cover (30% silt, 35% sand, 30% gravel, Plasticity Index Ip = 2–6%) from the lower alluvial deposit (15% silt, 20% sand, 65% gravel and cobbles). These data appear to be consistent with grain-size distribution ranges presented by Moser and Hohensinn (1983). Based on the results of in situ tests and on authors' experience on the characterization of local deposits, the friction angle of the soil cover (L1) was assumed equal to 36°–38°, while a 40°–42° friction angle was adopted for the lower alluvial well-graded deposit (L2). The shear properties of the unsaturated soil were determined according to the failure criterion proposed by Fredlund (2000), which extends the Mohr-Coulomb criterion to the unsaturated soil. The cohesion was neglected, and only the apparent cohesion due to the suction was accounted for. In order to estimate the apparent cohesion as a function of the water content, van Genuchten soil-water retention curves were used (see the following section for details). The unsaturated shear strength angle was computed according to the simplified model proposed by Vanapalli et al. (1996).

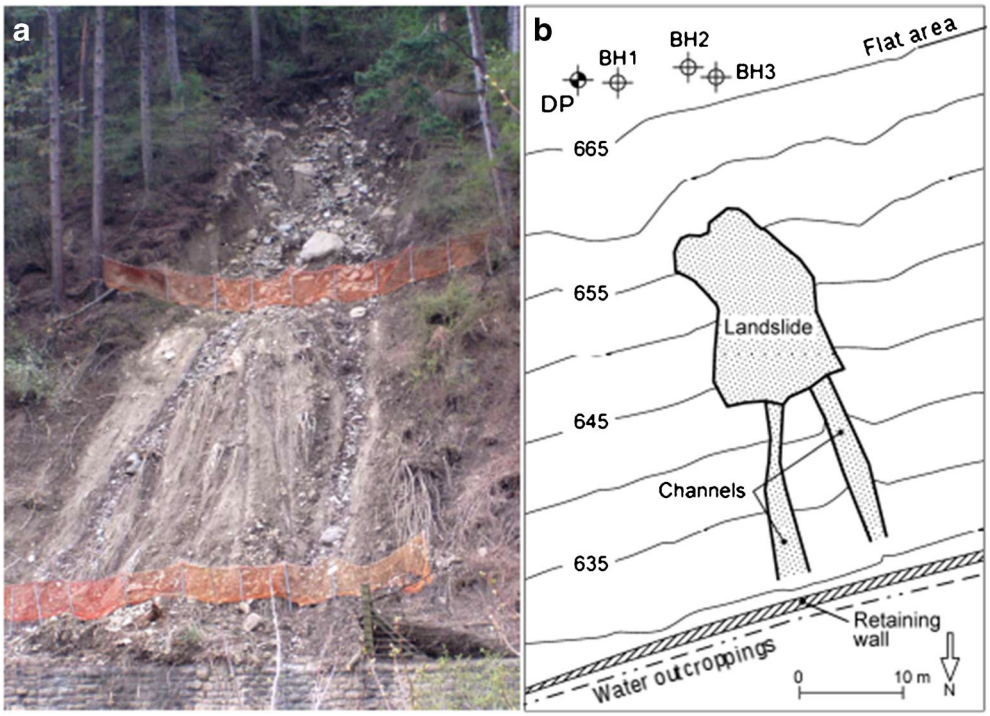

Fig. 1 **a**) View of the landslide and **b**) plan view of the hillslope with location of the landslide, of the discharge point (DP) and of the boreholes (BH) carried out during the investigation campaign following the event (after Sanzeni et al. 2017)

Hydrological properties

Lefranc tests allowed to estimate the hydraulic conductivity at saturation K_s of the layer L2 below the depth of 4.5 m. Measured K_s values ranged from 3.8×10^{-6} to 1.8×10^{-3} m/s, with smaller values in closer to the surface soil layers. For the purpose of the simulations, a representative conductivity of 1.5×10^{-4} m/s was adopted. Only grain size distribution curves and void ratios (ranging from 0.5 to 0.6) were available, and they were used to determine the parameters of the van Genuchten soil-water retention relationships and the characteristic water contents of the fine soil components (diameter smaller than 2 mm). For this purpose, pedotransfer functions implemented in the software Rosetta (Schaap et al. 2001) were applied. The estimated characteristic water content values were corrected for the presence of the soil skeletal fraction. The final set of soil-water retention curves parameters for layer L1 is the following: residual volumetric water content $\theta_r = 0.0246$ m^3/m^3, volumetric water content at saturation $\theta_s = 0.282$ m^3/m^3, scale factor $\alpha = 2.36$ 1/m, and shape factor $n = 1.41$ (with the usual constraint $m = 1–1/n$). For layer L2, they were respectively $\theta_r = 0.0213$ m^3/m^3, $\theta_s = 0.268$ m^3/m^3, $\alpha = 1.72$ 1/m, and $n = 1.43$ ($m = 1–1/n$). According to Rosetta's outputs, an equivalent conductivity at saturation ranging from 10^{-5} to 10^{-6} m/s for layer L1 seemed realistic. In the simulation process, after some trials, an equivalent value of $K_s = 7.50 \times 10^{-6}$ m/s was chosen. As no evidences of anisotropy were available, both L1 and L2 were considered isotropic. The

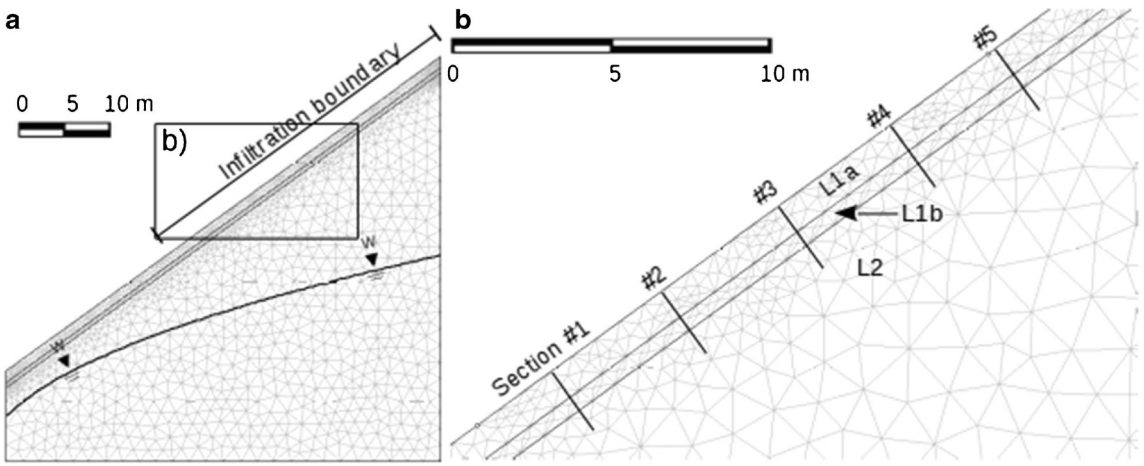

Fig. 2 **a**) Numerical model geometry. **b**) Detail

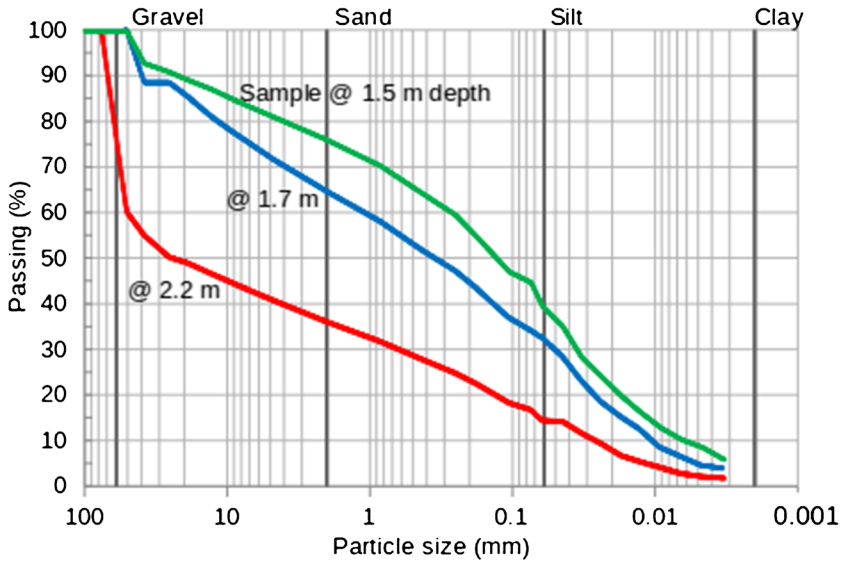

Fig. 3 Grain size distribution of soil samples from the hillside cover and from the alluvial deposit (after Sanzeni et al. 2017)

relative conductivity function was predicted with Mualem's model.

Such a two-layered soil model, with uniform and small conductivity at the uppermost layer, cannot lead to the formation of a perched water table. A perched water table in fact may onset within a soil laying on a capillary barrier, when the hydraulic conductivity (at soil saturation) continuously or sharply decreases with depth (Barontini et al. 2013). The transverse infiltration rate i_{pw}*, at which the perched water table is expected to onset, is related to the smallest value of the conductivity along the profile, $K_{s,min}$, and it is given by:

$$i_{pw}^{*} = K_{s,min} \cdot \cos\beta \tag{1}$$

where β is the slope of the hill. In terms of vertical infiltration i, which was used in the simulations, the previous equation becomes:

$$i_{pw} = K_{s,min} \tag{2}$$

The transverse infiltration rate for waterlogging, i_{wl}*, is related to the equivalent conductivity of the whole soil layer above the capillary barrier, $K_{s,eq}$, by:

$$i_{wl}^{*} = K_{s,eq} \cdot \cos\beta \tag{3}$$

The corresponding vertical infiltration, i_{wl}, is given by:

$$i_{wl} = K_{s,eq} \tag{4}$$

Two evidences suggested to identify two sublayers of L1: the presence of a rooted layer close to the soil surface (0.8 to 1.0 m deep) and the evidence of a superficial soil cover detected by elastic-acoustic surveys (0.5 to 1.0 m deep). Due to the root presence, the uppermost of these two sublayers (referred to as L1a) was supposed to have much greater conductivity than the other (L1b, Fig. 2b). For the simulation purposes, the values of $K_s = 2.55 \times 10^{-4}$ and 2.55×10^{-6} m/s were chosen for L1a and L1b, respectively, thus respecting the equivalent conductivity value of 7.50×10^{-6} m/s adopted for layer L1. Therefore, the minimal (vertical) infiltration rate i, which will lead to the onset of a perched water table, is 2.55×10^{-6} m/s. Since the conductivity profile, which preserves the equivalent conductivity of layer L1, affects the infiltration thresholds characterizing the onset of a perched water table, a number of different scenarios of conductivity profiles were explored to identify a possible range of minimal infiltration rates, which would lead to a perched water table in layer L1. The analysis was performed according to the criterion presented by Barontini et al. (2015), in which Zaslavsky's mapping (Zaslavsky 1964) of the conductivity at soil saturation is related to the perched water table properties. According to Zaslavsky's transformation, the transverse slope depth x* (null at the slope surface and positive entering the slope) is mapped in a new variable X* by the relationship:

$$dX^{*} = \frac{1}{K_s(x^{*})} dx^{*} \tag{5}$$

with $X^*(0) = 0$. Barontini et al. (2015) proved that, for a monotonically decreasing conductivity profile, a perched water table will onset when the transverse infiltration rate i_{pw}* is:

$$\frac{i_{pw}^{*}}{\cos\beta} > \left.\frac{dx^{*}}{dX^{*}}\right|_{bottom} \tag{6}$$

where dx^*/dX^* is calculated at the bottom of the investigated layer, just above the capillary barrier. The results of this analysis are reported in Fig. 4, where the dashed-dotted line represents Zaslavsky's mapping in the case of a uniform layer L1, and the other lines represent various combinations of layering and conductivities (in Fig. 4, *d1a* is the transverse depth of layer L1a, and *b* is the ratio between the conductivities of layer L1a and L1b). As a result of this analysis, values of (vertical) infiltration thresholds i_{pw}

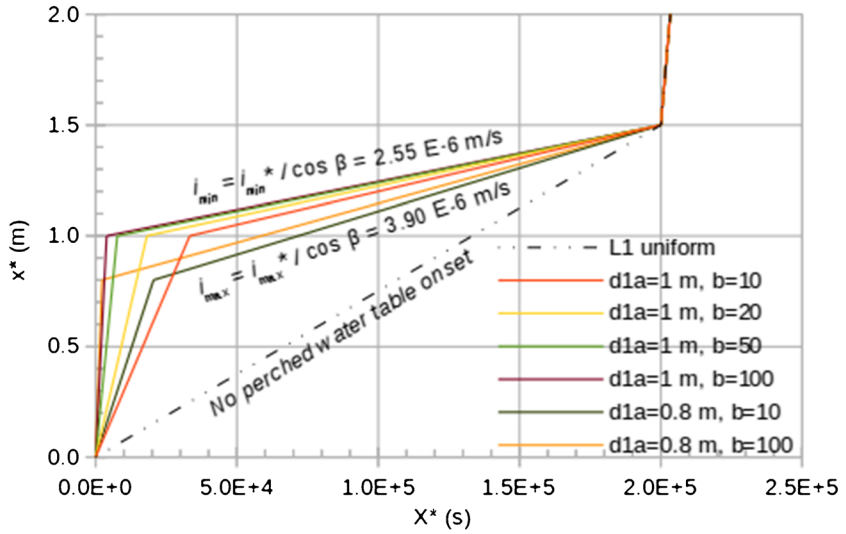

Fig. 4 Zaslavsky's mapping applied to determine the transverse infiltration thresholds i_{pw}*, leading to the onset of a perched water table in layer L1 (Eq. 6). Different scenarios of layering and conductivity profiles are presented ($d1a$ is the transverse depth of layer L1a; b is the ratio between the conductivities of layer L1a and layer L1b, respectively)

between 2.55×10^{-6} m/s and 3.90×10^{-6} m/s were found in all the investigated scenarios of soil layering.

Initial conditions

The soil-water content initial conditions were unknown, but a groundwater table at the depth of 22 m below the top of the slope was identified during the investigation campaign, and marks of water outcropping were recognized at the base of the slope (see Fig. 1b). Therefore, the depth of the groundwater in the central part of the slope ranges between 15 and 5 m. Under these circumstances, the groundwater table was represented with a Dupuit parabola which uncouples the unsteadiness of the simulation from the presence of the steady groundwater table flow (Fig. 2a). Within the unsaturated layer, hydrostatic initial conditions were applied in vertical direction, starting from the groundwater table (Fredlund 1997). This assumption implies that the surface soil-water potential in the interested area ranges between − 8 and − 15 m (Fig. 2a and Fig. 9a). Such pressure potentials are realistic for natural soils (Merrill and Rawlins 1972; Fredlund and Rahardjo 1993; Blight 2013), but in order to test how antecedent meteorological conditions might affect such pressure (and water content) distribution, a set of preliminary simulations was performed using Hydrus1D (Šimůnek et al. 2013). A simplified 1D, 3 layers and 3-m deep soil column, declined from the vertical direction as the investigated hillside, was set to mime the slope as an infinite uniform one. The three layers were 1.0 m (L1a), 0.5 m (L1b) and 1.5 m thick (L2), respectively. A hydrostatic distribution of the soil water pressure was assumed as initial condition, with two scenarios for the depth of the saturated layer, i.e. 3 m and 12 m below the soil surface, according to different positions of the groundwater table along the investigated slope. The temperature and precipitation measured at the nearby Schlanders/Silandro meteorological station in the 54 days before the event were used as boundary conditions. The relationship between root water uptake and pressure potential was taken into account in the simulation with Feddes' model (Feddes et al. 1978; Šimůnek et al. 2013). The result of these analyses indicated that most of the simulated water content dynamics were confined in the uppermost few decimetres of topsoil. Thus, the selected initial conditions in the unsaturated layer seemed realistic in the following 2D simulations.

Boundary conditions and simulations

The landslide was accidentally triggered by a great amount of water, estimated in the order of 10^{-2} m^3/s for a few hours, over an area ranging from 200 to 400 m^2, as assessed during the first site inspection immediately after the event. This would have produced an average infiltration rate between 10^{-5} and 10^{-4} m/s. As we were interested in testing the compatibility of a perched water table-induced failure mechanism with the available data, we explored two imbibition scenarios, either with assigned 2.55×10^{-4} m/s infiltration rate, or with assigned surface-soil pressure. The infiltration rate of 2.55×10^{-4} m/s, equal to K_s of layer L1a, is greater than the range of infiltration rates which would onset a perched water table without waterlogging (2.55×10^{-6} m/s < i < 7.50×10^{-6} m/s, see Eqs. 2 and 4) and was considered as an upper bound of the discharge that produced the collapse. The second scenario, with imposed surface soil pressure $p = 0$ kPa, was performed according to the idea that the amount of released water was so great that the surface soil affected by the infiltration might be practically and almost immediately led to saturation. The infiltration and soil saturation conditions were applied to two-thirds of the slope (Fig. 2a), as suggested by site inspection immediately after the event. The other boundary conditions were chosen in agreement with the steady initial conditions.

Results and discussion

Figure 5 presents six maps of pressure head computed with the infiltration boundary condition of 2.55×10^{-4} m/s applied over the upper two-thirds of the slope. In the maps, pressure-head values ranging from − 1.0 to + 1.0 m are represented (to appreciate the effect of infiltration; suction values are negative); the black-line contour represents the locus of zero pore-pressure

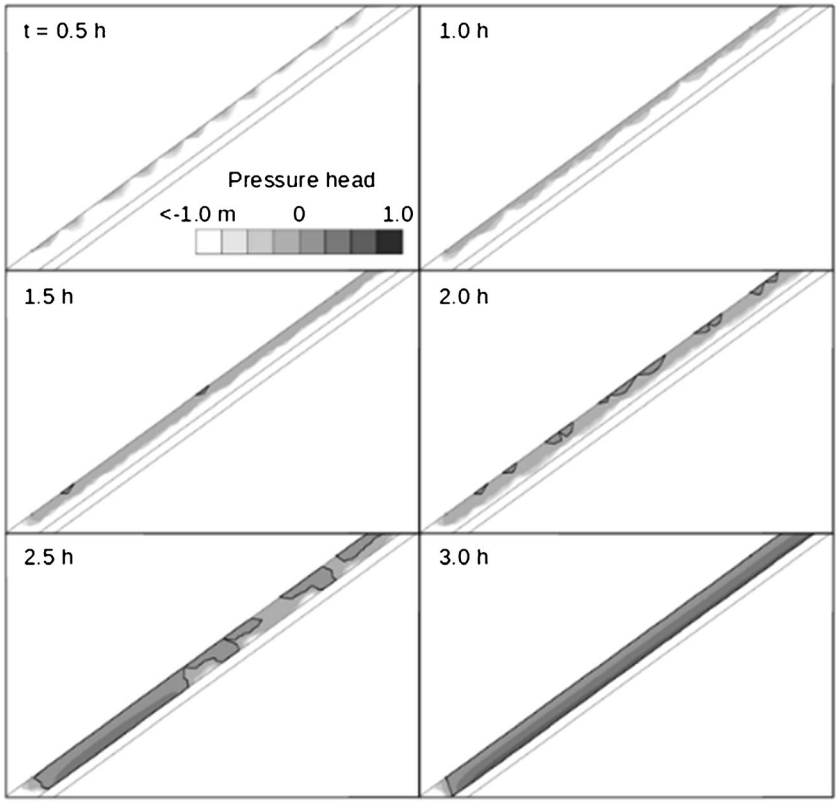

Fig. 5 Suction and pressure maps at 0.5, 1.0, 1.5, 2.0, 2.5 and 3.0 h from the beginning of the infiltration

points, and therefore, it identifies the extent of the perched water table. The imbibition process starts at the soil surface and rapidly develops involving the whole layer L1a within 3 h. According to the simulation, the perched water table initially appears between 1.5 and 2.0 h in the form of isolated patches that rapidly join in a single element with positive values of pore pressure at the interface between layer L1a and L1b. The pore pressure distribution during infiltration was adopted for the execution of stability analyses, and the main results are illustrated in Figs. 6 and 7. Figure 6 shows the centres of the slip surfaces with safety factor, SF, smaller than 1.2, and the surface with minimum SF, at 2.25 and 2.50 h from the beginning of the process. These instants were selected because they report the SF immediately before and after its dropdown. The instability area is located in the central part (i.e., the middle third) of the slope, which corresponds to the lower half of the area where the infiltration was applied; its extension is related to the amount of soil progressively involved in the process of

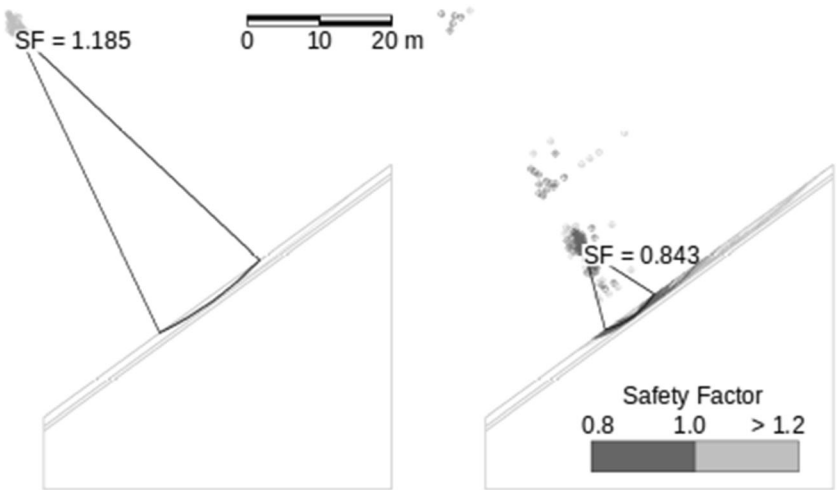

Fig. 6 Slip surfaces with safety factor smaller than 1.2, critical slip surfaces and minimum safety factors computed at 2.25 h (left) and 2.50 h (right) from the beginning of infiltration

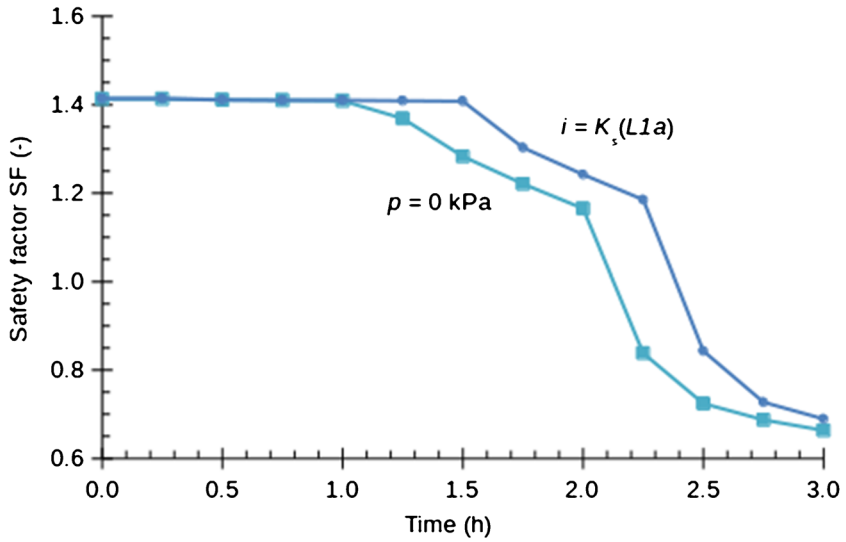

Fig. 7 Minimum safety factor SF estimated according to simplified Bishop method

formation of the perched water table. The position of the unstable area is in agreement with the documented field observations.

Figure 7 represents the SF evolution computed from two simulations executed with different boundary conditions applied over the upper two-thirds of the slope: (1) a maximum infiltration equal to 2.55×10^{-4} m/s; (2) a zero constant-pressure boundary condition. The value of SF during the initial stages of the infiltration is approximately 1.40; it starts decreasing as soon as the first patches of perched water table appear and it drops below unity when the patches join in a single perched water table with positive pore pressure. The simulation with zero constant-pressure leads to a faster crisis (SF = 1.0 between 2.10 and 2.15 h) compared to the maximum infiltration condition (SF = 1.0 between 2.35 and 2.40 h). The order of magnitude of the timing of the reconstructed crises is in agreement with the information collected after the event. According to the assumption that these two conditions may represent an upper bound of the discharged water, the estimated timing may be considered a lower bound of the timing of the event.

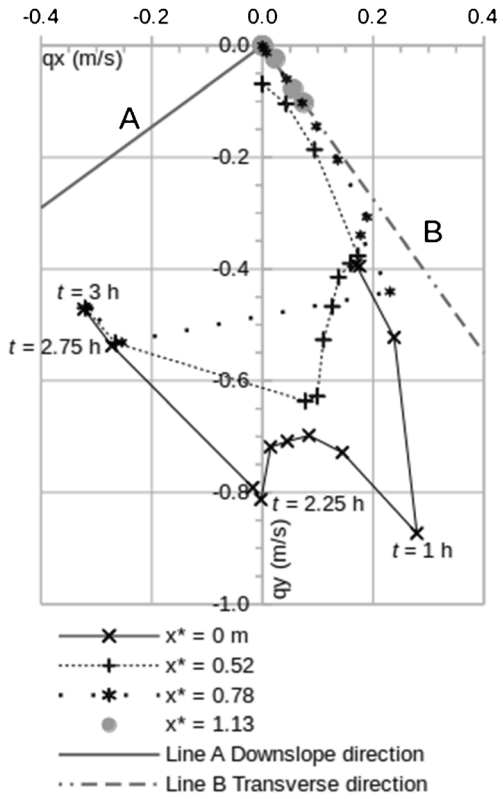

Fig. 8 Evolution of flux direction during the imbibition process

In Figs. 8 and 9, some details of the hydrological processes are presented for zero pressure condition. Figure 8 shows the evolution of the flow regime along a midway transverse section where the perched water table appears. The figure represents the vertical component q_y of the Darcian fluxes plotted against the horizontal one q_x, for different depths x^*, and at different time steps. Line A represents the downslope direction (parallel to the slope inclination), and line B represents the transverse direction (normal to the slope inclination). At the beginning of the infiltration, the fluxes are markedly transverse and lay close to line B. These fluxes are mainly diffusive and driven by the gradients of the soil suction. As the infiltration progresses, the corresponding change in water content and in conductivity allows also advective fluxes to onset. Thus, the direction of the flux migrates towards line A. The direction of line A is not reached because even when the perched water table is formed, there is still a transverse component of the Darcian flux in layer L1a. It is worth noting that when the crisis occurs, layer L1b is still minimally affected by the imbibition process, and the fluxes at depth $x^* = 1.13$ m follow the transverse direction.

Figure 9a illustrates the evolution of the suction and pressure head along four transverse sections across the central third of the slope. The plot shows that a perched water table appears at the interface between the more conductive soil layer L1a ($x^* <$ 1 m) and the less conductive L1b (1 m $< x^* <$ 1.5 m). The perched water table is recognized after 2.0 h (x^* smaller than 0.5 m), and the soil is waterlogged at 3.0 h, with positive pore pressure. As

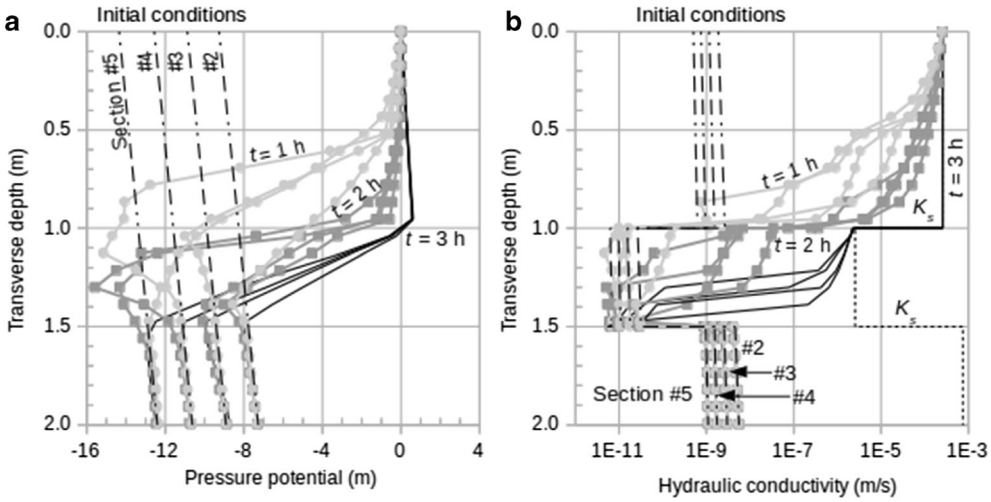

Fig. 9 **a**) Pressure potential evolution along a series of transverse sections across the perched water table responsible of the dropdown of the safety factor. **b**) Water conductivity evolution along a series of transverse sections across the perched water table responsible of the dropdown of the safety factor

already computed by Peli et al. (2012), once the perched water table onsets, then it rapidly reaches steady conditions. Figure 9b represents the conductivity profiles across the same transverse sections and at the same instants. The dotted line (on the right side of the plot) represents the profile of the hydraulic conductivity at soil saturation K_s, which is reached by all the points in layer L1a at 3 h, thus confirming that soil saturation is reached and that the layer is waterlogged. At the same time, layer L2 is still not affected by the infiltration process, which remains confined in L1a and L1b. Layer L2 thus behaves as a capillary barrier.

As already mentioned, the applied infiltration rate should be considered as an upper bound of the discharged water. Therefore, other scenarios with smaller infiltration rates, over the upper two-thirds of the slope, were investigated to appreciate the model response. The results are plotted in Fig. 10, which represents the crisis time (when SF = 1) as a function of the infiltration rate, to reconstruct a pseudo-intensity-duration function (pseudo-IDf). The obtained pseudo-IDf is well interpolated by the power function $i = 1.63\ t^{-0.84}$ (m/h). If compared with other literature cases of IDfs (Moser and Hohensinn 1983; Cancelli and Nova 1985; Guzzetti et al. 2008), the obtained infiltration values are very great as the landslide was triggered by an exceptional amount of water in an otherwise stable slope.

Conclusions

A landslide event, which occurred in Northern Italy in April 2010, accidentally triggered by an unexpected and extraordinary

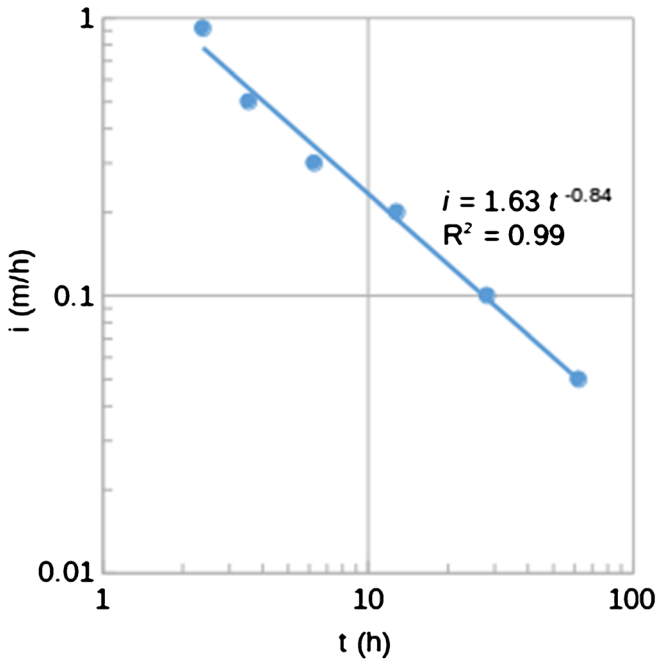

Fig. 10 Time of collapse as a function of infiltration intensity over the upper two-thirds of the slope model

soil imbibition, was modelled to understand the possible failure mechanism. After collecting and analysing the available data, it seemed realistic that the triggering mechanisms was the onset of a perched water table in the uppermost soil layers and below the rooted soil. In order to test this hypothesis, the hydrologic soil properties (with van Genuchten-Mualem constitutive laws) were inferred with Rosetta software, based on the available grain-size distribution curves. Then, a number of uncoupled hydrologic and stability 2D simulations were carried out with a commercial computer software. Regarding the hydrological model, the evidence of a rooted layer close to the soil surface suggested to split the superficial soil into two sublayers, the uppermost of which was supposed to have much greater conductivity than the other one. A number of different scenarios of conductivity profiles was explored to identify a possible range of the minimal infiltration rates, which would lead to a perched water table. As a result of this analysis, comparable values of infiltration thresholds were found in all the investigated scenarios and a ratio between conductivities at soil saturation of 100 seemed realistic for the simulations. The modelling strategy was based on the idea of representing a steady groundwater table within the slope, shaped as a Dupuit parabola. A vertically hydrostatic pore pressure distribution was imposed as initial condition for the vadose zone. A preliminary 1D analysis of the water balance of the uppermost soil layers during the 54 days before the event suggested that, in any case, most of the hydrologic dynamics occurred within the rooted soil layer. Two imbibition scenarios were explored: one with maximum infiltration rate equal to the saturated conductivity of the uppermost soil sublayer; the other with assigned surface-soil pressure $p = 0$ kPa. These conditions were applied to two-thirds of the slope and were intended to represent an upper bound of the discharged water.

The simulations effectively reproduced the formation of a perched water table in the central part of the modelled slope. The imbibition process rapidly developed involving the most superficial soil within 3 h. A perched water table initially appeared between 1.5 and 2.0 h in the form of isolated patches that rapidly joined in a single element, at the interface between the two soil sublayers (1.0 m depth). The imbibition process remained confined in the uppermost layers, and the coarse and deeper soil deposit behaved as a capillary barrier. The resulting pore pressure regime affected the slope stability, with values of the safety factor rapidly decreasing as the imbibition progressed. The initial value of SF was approximately 1.40 and dropped below unity when the patches of saturated soil joined. The order of magnitude of the timing of the reconstructed crises appeared to be in agreement with the information collected after the event. According to the assumption that these two conditions may represent an upper bound of the discharged water, the estimated timing may be considered a lower bound of the timing of the event.

Finally, other scenarios with smaller infiltration rates were investigated to appreciate the model response and a pseudo-intensity-duration function was reconstructed. The infiltration values of the pseudo-IDf were great in comparison to other literature IDfs, as a demonstration that the landslide was triggered by an exceptional amount of water in an otherwise stable slope.

References

Askarinejad A, Casini F, Bischof P, Beck A, Springman SM (2012) Rainfall induced instabilities: a field experiment on a silty sand slope in northern Switzerland. Riv Ital Geotec 3:50–71

Barla G, Antolini F, Barla M (2013) Slope stabilization in difficult conditions: the case study of a debris slide in NW Italian Alps. Landslides. 10:343–355

Barontini S, Peli M, Bogaard T A, Ranzi R (2013) Dimensionless numerical approach to perched waters in 2D gradually layered soils. In: Margottini C, Canuti P, Sassa K (eds) Landslide science and practice. Volume 3: Spatial analysis and modelling, pp. 143–149

Barontini S, Falocchi M, Ranzi R (2015) Steady lateral flow in sloping soils: which is the effect of the conductivity at saturation profile? In: Lollino G, Giordan D, Crosta GB, Corominas J, Azzam R, Wasowski J, Sciarra N (eds) Engineering geology for society and territory. Volume 2: Landslide processes, pp. 2153–2156

Bishop AW (1955) The use of the slip circle in the stability analysis of slopes. Géotechnique 5:7–17

Blight GE (2013) Unsaturated soil mechanics in geotechnical practice. CRC Press/Balkema

Bogaard TA, Greco R (2016) Landslide hydrology: from hydrology to pore pressure. Wiley Interdiscip Rev Water 3(3):439–459

Bogaard TA, Greco R (2018) Hydrological perspectives on precipitation intensity-duration thresholds for a landslide initiation: proposing hydro-meteorological thresholds. Nat Hazards Earth Syst Sci 18(1):31–39

Caine N (1980) The rainfall intensity-duration control of shallow landslides and debris flows. Geogr Ann Ser A, Phys Geography 62(1–2):23–27

Cancelli A, Nova R (1985) Landslides in soil debris cover triggered by rainstorms in Valtellina (Central Alps – Italy). In: Sassa LK (ed) Proceedings of the 4th international conference and field workshop on landslides, Tokyo, pp 267–272

Cascini L, Cuomo S, Pastor M, Sorbino G (2010) Modeling of rainfall-induced shallow landslides of the flow-type. J Geotech Geoenviron Eng 136(1):85–98

Cascini L, Cuomo S, Della Sala M (2011) Spatial and temporal occurrence of rainfall-induced shallow landslides of flow type: a case of Sarno-Quindici, Italy. Geomorphology 126:148–158

Feddes RA, Kowalik PJ, Zaradny H (1978) Simulation of field water use and crop yield. John Wiley and Sons, New York (NY)

Fredlund DG (1997) An introduction to unsaturated soil mechanics. In: Houston SL and Fredlund DG (eds) Unsaturated soil engineering practice. ASCE, Geotech Spec Publ 68:1–37

Fredlund DG (2000) The 1999 R.M. hardy lecture: the implementation of unsaturated soil mechanics into geotechnical engineering. Can Geotech J 37:963–986

Fredlund DG, Rahardjo H (1993) Soil mechanics for unsaturated soils. John Wiley & Sons Inc.

Guzzetti F, Perucacci S, Rossi M, Stark CP (2008) The rainfall intensity-duration control of shallow landslides and debris flow: an update. Landslides 5:3–17

Khire M, Benson C, Bosscher P (2000) Capillary barriers in semi-arid and arid climates: design variables and the water balance. J Geotech Geoenviron Eng 126(8):695–708

Mancarella D, Doglioni A, Simeone V (2012) On capillary barrier effects and debris slide triggering in unsaturated layered covers. Eng Geol 147-148:14–27

Merrill SD, Rawlins SL (1972) Field measurement of soil water potential with thermocouple psychrometers. Soil Sci 113(2):102–109

Moser M, Hohensinn F (1983) Geotechnical aspects of soil slips in alpine regions. Eng Geol 19(3):185–211

Ozbay A, Cabalar AF (2015) FEM and LEM stability analysis of the fatal landslides at Çöllolar open-cast lignite mine in Elbistan, Turkey. Landslides 12:155–163

Peli M, Barontini S, Bogaard TA, Bacchi B, Ranzi R (2012) Non monotonic imbibition profiles and transition to a perched water table in a gradually layered soil. In: Mancuso C, Jommi C and D'Onza F (eds) Unsaturated soils: research and applications, proceedings of the 2nd European conference on unsaturated soils, 2:167–174

Rocscience Inc. (2010) SLIDE version 6.0-2D limit equilibrium slope stability analysis. Toronto, Ontario (www.rocscience.com)

Sanzeni A, Cancelli T, Peli M, Barontini S, Colleselli F (2017) Back-analysis of an artificially triggered landslide: a case study in Northern Italy. In: Mikoš M, Tiwari B, Yin Y, Sassa K (eds) Advancing culture of living with landslides. Vol. 2: Advances in landslide science, Set 1. Springer International Publishing, pp. 541–549

Schaap MG, Leij FJ, van Genuchten MTh (2001) Rosetta: a computer program for estimating soil hydraulic parameters with hierarchical pedotransfer functions. J Hydrol 251:163–176

Shackelford CD, Chang CK, Chiu TF (1994) The capillary barrier effect in unsaturated flow through soil barriers. In: Proceedings of the First International Congress on Environmental Geotechnics, Edmonton, Canada, pp. 789–793

Šimůnek J, Šejna M, Saito H, Sakai M, van Genuchten MTh (2013) The Hydrus-1D Software Package for simulating the movement of water, heat, and multiple solutes in variably saturated media. Version 4.17, HYDRUS Software Series 3, Department of Environmental Sciences, University of California Riverside, Riverside, California, USA

Springman SM, Thielen A, Keinzler P, Friedel S (2013) A long-term field study for the investigation of rainfall-induced landslides Géotechnique. 63(14):1177–1193

Tarantino A, Bosco G (2000) Role of soil suction in understanding the triggering mechanisms of flow slides associated with rainfall. In: Wieczorek GF and Naeser ND (eds) Debris-Flow Hazard Mitigation, Proceeding of the 2nd International Conference on debris-flow hazard mitigation, Taipei, Taiwan. Balkema, pp. 81–88

Vanapalli SK, Fredlund DG, Pufahl DE, Clifton AW (1996) Model for the prediction of shear strength with respect to soil suction. Can Geotech J 33:379–392

Zaslavsky D (1964) Theory of unsaturated flow into a non-uniform soil profile. Soil Sci 97(6):400–410

A. Sanzeni (✉) · M. Peli · S. Barontini · F. Colleselli
DICATAM,
Università degli Studi di Brescia,
Via Branze, 43, 25123, Brescia, Italy
Email: alex.sanzeni@unibs.it

M. Peli
e-mail: marco.peli@unibs.it

S. Barontini
e-mail: stefano.barontini@unibs.it

F. Colleselli
e-mail: francesco.colleselli@unibs.it